Adaptive Robust Control of Atmospheric Pressure Plasma Jets in Linear Parameter-varying Framework

Pegah GhafGhanbari¹ and Javad Mohammadpour Velni¹

Abstract—Atmospheric pressure plasma jets (APPJs) hold significant promise in biomedical applications, where safe and efficient operation is critical. In this study, a new data-driven robust control paradigm is proposed for APPJs in the Linear Parameter-varying (LPV) framework. By leveraging Bayesian Neural Networks (BNNs), a state space LPV model is identified to capture the intricate nonlinear dynamics of APPJs while providing statistical insights into the system's behavior. This approach allows for the adaptation of the uncertainty region at each time step, enhancing closed-loop control adaptability, and alleviating the conservativeness of the control design compared to the conventional robust controllers. The proposed robust Model Predictive Control (MPC) design method operates through an online process, where an optimization problem, formulated using Linear Matrix Inequalities (LMIs), computes a time-varying feedback control law. Through extensive simulations, the LPV-based robust control's efficacy in handling modeling discrepancies and external disturbances is assessed. Furthermore, a comparison is made with an alternative control scheme employing MPC with a given LTI model, demonstrating the superior robustness and tracking capabilities of the proposed LPV-MPC-based approach. These findings underscore the potential of the proposed technique to enhance APPJ control across diverse practical scenarios.

I. INTRODUCTION

Atmospheric Pressure Plasma Jets (APPJs) represent a class of cold plasma devices known for precise delivery of localized physical and chemical effects onto intricate surfaces [1]. Operating in a non-equilibrium regime with electron temperatures typically ranging from 1 to 5 electron volts (eV) while the background gas remains at around room temperature [2], they offer significant promise for treating heat- and pressure-sensitive surfaces in materials processing [3], [4] and biomedical applications [5].

APPJs consist primarily of a dielectric capillary tube through which noble gases like helium (He) or argon (Ar) flow. An enclosed electrode system applies an electric field to the gas flow, initiating plasma formation. The resulting plasma *plume*, extending several centimeters from the tube's end or nozzle, acts as an active zone for surface treatment. APPJs also draw in ambient gas as they emanate from the nozzle, fostering a dynamic mixture of gases and facilitating chemical reactions, generating various reactive species[6].

The intricate dynamics and modeling uncertainties intrinsic to these devices, along with their sensitive applications, pose significant challenges for control design. Gidon et al.

[7] proposed a lumped-parameter, physics-based model to characterize APPJ dynamics and employ it for MPC design. However, the inherent assumptions limit the incorporation of intricate system dynamics, making the system and controller vulnerable to uncertainties. Data-driven methods, like subspace identification, offer an alternative for model identification. Yet, resulting linear time-invariant (LTI) models often fall short in capturing the full nonlinear dynamics. In response, Bao et al. [8] introduced Bayesian Neural Networks (BNNs) to address modeling mismatches, generating uncertain scenarios for scenario-based MPC design.

The Linear Parameter-varying (LPV) modeling framework provides flexibility in representing nonlinear dynamic systems, capturing dependencies on varying parameters called scheduling variables. It enables the use of common linear control synthesis tools and facilitates model-based controller design for systems with nonlinear and time-varying behavior [9]. In a recent study by Gidon et al. [1], a data-driven LPV input—output (IO) representation of the APPJ was developed and used in a supervisory MPC scheme to regulate nonlinear thermal effects of plasma on a surface. Despite the LPV framework's modeling flexibility, uncertainties in data, systems, and optimization processes often lead to plant-model mismatch [10]. Hence, robust control strategies that explicitly address uncertainties and modeling discrepancies are crucial to ensure system stability and performance.

Robust control methods can address this challenge by explicitly considering uncertainties in system dynamics. They integrate a priori estimates of model uncertainty into controller design, ensuring stability and performance across all modeled uncertainties. However, traditional approaches often maintain a static uncertainty estimate during operation, potentially compromising overall controller performance by optimizing objectives across all conceivable models within the uncertainty specification [11].

This paper presents a data-driven robust MPC strategy within the LPV framework to mitigate uncertainties in AP-PJs. By utilizing BNNs for system identification, the method captures intricate system dynamics and statistical properties, offering insights into modeling uncertainty. Through robust control design techniques, the approach optimizes controller performance while ensuring stability under varying operating conditions and typical uncertainties in APPJs. Unlike conventional robust control methods relying on worst-case scenarios, this work dynamically calculates uncertainty at each time instant, enhancing system performance and mitigating conservatism. This methodology shows promise for enhancing APPJ control, providing heightened performance

^{*}This work was supported by the US National Science Foundation under award #2302219.

¹Authors are with the Dept. of Mechanical Engineering, Clemson University, Clemson, SC 29634, USA. E-mail addresses: {pghafgh, javadm}@clemson.edu.

and adaptability to the dynamic and uncertain nature of plasma jet systems.

The paper is organized as follows: Section II introduces the problem formulation, while Section III addresses the data-driven system identification problem. Section IV follows by extracting the uncertain system model, leading into Section V, which elaborates on the proposed robust control methodology. Section VI presents simulation results and discussions, and Section VII concludes the paper.

II. PROBLEM FORMULATION

A lumped-parameter, discrete-time nonlinear model of APPJs can be expressed as

$$x(k+1) = f(x(k), u(k)),$$
 (1a)

$$y(k) = h(x(k), u(k)), \tag{1b}$$

where x(k), u(k), and y(k) are the state, input, and output vectors at time instant $k \in \mathbb{N}$. Moreover, $f: \mathbb{R}^{n_x} \times \mathbb{R}^{n_u} \mapsto \mathbb{R}^{n_x}$ and $h: \mathbb{R}^{n_x} \times \mathbb{R}^{n_u} \mapsto \mathbb{R}^{n_y}$ represent the dynamic and measurement models, respectively. The nonlinear dynamic model, f(x(k), u(k)), can be represented by an LPV-state space (LPV-SS) model structured as (2). This allows for the adoption of a linear control framework while simultaneously improving model precision across a wide range of operating conditions. The LPV-SS model is written as,

$$x(k+1) = A(p(k))x(k) + B(p(k))u(k),$$
 (2a)

$$y(k) = C(p(k))x(k) + D(p(k))u(k),$$
 (2b)

where $A: \mathbb{R}^{n_p} \mapsto \mathbb{R}^{n_x \times n_x}$, $B: \mathbb{R}^{n_p} \mapsto \mathbb{R}^{n_x \times n_u}$, $C: \mathbb{R}^{n_p} \mapsto \mathbb{R}^{n_y \times n_x}$, and $D: \mathbb{R}^{n_p} \mapsto \mathbb{R}^{n_y \times n_u}$ denote state, input, output, and feedforward matrices, which are functions of time-varying scheduling variables $\mathrm{p}(k) \in \mathbb{R}^{n_p}$. In this study, the state-space matrices are learned using Bayesian neural networks, as elaborated in the subsequent section.

III. DATA-DRIVEN SYSTEM IDENTIFICATION

This section explores system identification/learning within the LPV framework, employing Bayesian Neural Networks (BNNs) to capture complex system dynamics probabilistically, without strict reliance on explicit mathematical or physical models. Unlike Artificial Neural Networks (ANNs), which are prone to outliers and overfitting, BNNs excel in capturing intricate behaviors while quantifying uncertainty in model identification [12]. Integrating uncertainty into the modeling process, the BNN-based LPV model learning offers a superior approximation of underlying system dynamics using experimental observations.

The uncertainty inherent in BNN model structure emerges from treating the parameters of the neural network as random variables and assigning prior distributions as a scaled mixture of two Gaussian distributions as [13],

$$p(\mathbf{w}_{i}) = \rho_{\mathbf{m}, i} \mathcal{N}(\mathbf{w}_{i} | 0, \sigma_{i, 1}^{2}) + (1 - \rho_{\mathbf{m}, i}) \mathcal{N}(\mathbf{w}_{i} | 0, \sigma_{i, 2}^{2}), (3)$$

where the tuning parameter $\rho_{m,j}$ serves as the regulator for the prior density of the parameters in the j-th layer of the neural network, denoted as w_j . Larger values of $\sigma_{j,1}$ lead to

heavier-tailed distributions, whereas smaller values of $\sigma_{j,2}$ result in more concentrated ones. Utilizing cross-validation enables finding these parameters [14].

Through training, the posterior distribution over network parameters, given dataset \mathcal{D} , is estimated using variational inference (VI) techniques, which approximate complex probability distributions by selecting a member from a family of densities that closely approximates the target distribution, minimizing the Kullback-Leibler (KL) divergence between the true posterior distribution and the approximation [15]. To approximate the posterior $p(\mathbf{w}_i|\mathcal{D})$, VI solves

$$\min_{\theta_{j}} KL\left(q(\mathbf{w}_{j}; \theta_{j})||p(\mathbf{w}_{j}|\mathcal{D})\right) \tag{4a}$$

$$\Leftrightarrow \min_{\theta_{j}} KL\left(q(\mathbf{w}_{j}; \theta_{j})||p(\mathbf{w}_{j})\right) - \mathbb{E}_{q(\mathbf{w}_{j}; \theta_{j})}[\log p(\mathbf{w}_{j}|\mathcal{D})]$$

$$\Leftrightarrow \min_{\theta_{j}} \left(\mathbb{E}_{q(\mathbf{w}_{j}; \theta_{j})}[\log q(\mathbf{w}_{j}; \theta_{j})] - \mathbb{E}_{q(\mathbf{w}_{j}; \theta_{j})}[\log p(\mathbf{w}_{j})]$$

$$- \mathbb{E}_{q(\mathbf{w}_{j}; \theta_{j})}[\log p(\mathcal{D}|\mathbf{w}_{j})]\right), \tag{4b}$$

where $q(\mathbf{w}_j;\theta_j)$ represents a family of densities parameterized by θ_j . The evidence lower bound (ELBO) function, as defined in (4b), is optimized using Monte Carlo (MC) methods and backpropagation [15]. The distribution $q(\mathbf{w}_j;\theta_j)$ is parameterized as $\mathbf{w}_j = \mu_j + \sigma_j \odot \varepsilon_j$, where \odot denotes element-wise multiplication, $\varepsilon_j \sim \mathcal{N}(0,I)$, and $\theta_j = (\mu_j,\sigma_j)$ (note that μ and σ denote the mean and standard deviation, respectively, and \mathcal{N} is the normal distribution). Subsequently, the BNN is trained by solving the following optimization problem over θ using the dataset \mathcal{D}

$$\min_{\theta} \frac{1}{n_b} \sum_{i=1}^{n_b} [\log q(\mathbf{w}^{(i)}; \theta) - \log p(\mathbf{w}^{(i)}) - \log p(\mathcal{D}|\mathbf{w}^{(i)})],$$
(5)

where $\mathbf{w}^{(i)}$ represents the *i*-th sample generated by MC to approximate the ELBO, and n_b denotes the MC sample size chosen to ensure convergence to a local optimum for (5).

The BNN-based LPV-SS model identification problem involves learning matrices $A(\mathbf{p}_k)$ and $B(\mathbf{p}_k)$ from a training dataset $\mathcal{D} = \{(\mathbf{p}(i), x(i), u(i)), (x(i+1))\}_{i=0}^{N-1}$. Using the trained BNNs, the density of the matrix functions at a given scheduling variable is assessed by drawing n_{MC} samples from the posteriors of weights, leading to the calculation of potential matrices with each set of sampled weights. Rather than directly estimating the density from samples, the statistics such as the mean and standard deviation of each matrix element is calculated. This approach proves to be both efficient and adequate for constructing a confidence interval of state-space matrices.

Assuming that all states are measurable, the C matrix will be constant and the nominal value of matrices A and B, and their corresponding standard deviations are calculated as

$$\bar{A}(k) = \frac{1}{n_{\text{MC}}} \sum_{i=1}^{n_{\text{MC}}} A^{(i)}, \quad \bar{B}(k) = \frac{1}{n_{\text{MC}}} \sum_{i=1}^{n_{\text{MC}}} B^{(i)}$$
 (6)

$$\sigma^{A}(k) = \sqrt{\frac{1}{n_{\text{MC}}} \sum_{i=1}^{n_{\text{MC}}} (A^{(i)} - \bar{A}(k))^{\top} (A^{(i)} - \bar{A}(k))}$$
 (7a)

$$\sigma^{B}(k) = \sqrt{\frac{1}{n_{\text{MC}}} \sum_{i=1}^{n_{\text{MC}}} (B^{(i)} - \bar{B}(k))^{\top} (B^{(i)} - \bar{B}(k))}$$
 (7b)

IV. SYSTEM DESCRIPTION IN POLYTOPIC FORM

The LPV-SS model obtained in the previous section can be presented in the following *polytopic* or *multi-model* form

$$x(k+1) = A(p(k))x(k) + B(p(k))u(k),$$
 (8a)

$$y(k) = Cx(k), (8b)$$

$$[A(\mathbf{p}(k)) \ B(\mathbf{p}(k))] \in \Omega(k).$$

The set Ω is a polytope defined by,

$$\Omega(k) = \text{Co}\{[\hat{A}_1(k) \ \hat{B}_1(k)], \dots, [\hat{A}_r(k) \ \hat{B}_r(k)]\}$$
 (9)

where $\operatorname{Co}\{.\}$ indicates that the set $\Omega(k)$ is a convex hull. This implies that for some non-negative λ_i 's, $\sum_{i=1}^r \lambda_i = 1$, the following holds

$$[A(p(k)) \ B(p(k))] = \sum_{i=1}^{r} \lambda_i [\hat{A}_i(k) \ \hat{B}_i(k)]. \tag{10}$$

To form $\Omega(k)$ at each time step, the combinations of the boundaries of the confidence interval for A(p(k)) and B(p(k)) are chosen as

$$\Omega = \operatorname{Co}\{[\bar{A}(k) + \beta \sigma^{A}(k) \ \bar{B}(k) + \beta \sigma^{B}(k)],$$

$$[\bar{A}(k) + \beta \sigma^{A}(k) \ \bar{B}(k) - \beta \sigma^{B}(k)],$$

$$[\bar{A}(k) - \beta \sigma^{A}(k) \ \bar{B}(k) + \beta \sigma^{B}(k)],$$

$$[\bar{A}(k) - \beta \sigma^{A}(k) \ \bar{B}(k) - \beta \sigma^{B}(k)]\}, \quad (11)$$

where β is a tuning parameter that determines the width of the confidence interval.

V. LMI-BASED ROBUST CONTROL DESIGN METHOD

In this section, we present the development of an LMIbased robust control law tailored to address the reference tracking challenges inherent in complex dynamic systems including APPJs.

Assumption 1: The dynamics of the reference trajectory can be described by [16]

$$x_r(k+1) = A_r(k)x_r(k),$$
 (12a)

$$y_r(k) = C_r(k)x_r(k). (12b)$$

This form of the reference trajectory has the capability to generate a diverse set of command trajectories, encompassing useful patterns such as step, sinusoidal waveforms, ramp, and various other patterns [17].

Utilizing the system dynamics given by (8) and the reference dynamics (12), we formulate an augmented state-space model for the system as

$$\mathcal{X}(k+1) = \mathcal{A}(p(k))\mathcal{X}(k) + \mathcal{B}(p(k))\Delta u(k)$$
 (13a)

$$y = \mathcal{CX}(k) \tag{13b}$$

$$\mathcal{A} = \begin{bmatrix} A(\mathbf{p}(k)) & 0 & B(\mathbf{p}(k)) \\ 0 & A_r(k) & 0 \\ 0 & 0 & I \end{bmatrix}, \quad \mathcal{B} = \begin{bmatrix} B(\mathbf{p}(k)) \\ 0 \\ I \end{bmatrix},$$

$$C = \begin{bmatrix} C & 0 & 0 \end{bmatrix}, \qquad [A(p(k)) & B(p(k))] \in \Omega,$$

 $\mathbf{\Omega} = \text{Co}\{ [\hat{\mathcal{A}}_1(k) \ \hat{\mathcal{B}}_1(k)], [\hat{\mathcal{A}}_2(k) \ \hat{\mathcal{B}}_2(k)], \dots, [\hat{\mathcal{A}}_r(k) \ \hat{\mathcal{B}}_r(k)] \}$

where the augmented state, denoted as $\mathcal{X}(k) = [x^T(k) \ x_r^T(k) \ u^T(k-1)]^T$, encompasses the original states and their reference counterparts at time k, as well as the control inputs at the previous time step, k-1. Additionally, $[\hat{\mathcal{A}}_i(k) \ \hat{\mathcal{B}}_i(k)], \ i \in \{1,\ldots,r\}$ denotes the i^{th} vertex of the polytopic uncertainty inherent in the augmented system, and I denotes the identity matrix.

Given the i-step-ahead prediction of augmented state vector at time instant k, the tracking error can be estimated as

$$e(k+i|k) = C_e \mathcal{X}(k+i|k),$$

$$C_e = \begin{bmatrix} C & -C_r & 0 \end{bmatrix}.$$
(14)

Therefore, the error dynamics can be written as

$$e(k+i+1|k) = C_e \mathcal{A}(p(k)) \mathcal{X}(k+i|k) + C_e \mathcal{B}(p(k)) \Delta u(k+i|k).$$
 (15)

Our primary control objective is to optimize system performance while ensuring robustness against uncertainties. This objective is formulated using the following optimization problem as described in [18], tailored for tracking task.

$$\min_{u(k+i|k),i=0,1,...,m} \max_{[\hat{\mathcal{A}}(k) \ \hat{\mathcal{B}}(k)] \in \Omega} J_{\infty}(k) \tag{16a}$$

$$J_{\infty}(k) = \sum_{i=0}^{\infty} \left(\|e(k+i|k)\|_{Q_1}^2 + \|\Delta u(k+i|k)\|_R^2 \right). \tag{16b}$$

Here, $Q_1 \succeq 0$ and $R \succ 0$ represent penalty weights, while $\Delta u(k+i|k)$ denotes predicted control input variations at time k+i based on measurements at time k. Solving the min-max optimization problem described above presents computational challenges. Therefore, following the approach outlined in [18], we initially establish an upper bound γ on the robust performance objective, $J_{\infty}(k) < \gamma$.

Subsequently, we minimize this upper bound using a feedback control law $\Delta u(k+i|k) = Ke(k+i|k)$. To do so, we choose a quadratic Lyapunov function as

$$V(e(k|k)) = e^{T}(k|k)Pe(k|k), P \succ 0$$
(17)

with $e(\infty|k)=0$, and V(0)=0. To guarantee the decreasing nature of γ , the following inequality must be satisfied

$$V(e(k+i+1|k)) - V(e(k+i|k)) \le - [e(k+i|k)^{T} Q_{1} e(k+i|k) + \Delta u(k+i|k)^{T} R \Delta u(k+i|k)].$$
(18)

Summing (18) over $i = \{0, 1, ..., \infty\}$ results in

$$-V(e(k|k)) \le -J_{\infty}(k),\tag{19}$$

which implies that

$$\max_{[\mathcal{A}(k) \ \mathcal{B}(k)] \in \Omega} J_{\infty}(k) \le V(e(k|k)) \le \gamma. \tag{20}$$

Therefore, it can be concluded that the Lyapunov function (17) serves as an upper bound for the robust objective function (16b).

Theorem 1: [16] Suppose that the uncertainty set Ω is defined by a polytope as described in (13). In this scenario, the feedback control law $\Delta u(k+i|k)=Ke(k+i|k),\ i\geq 0$, with the feedback gain $K=YQ^{-1}$ minimize the upper bound of the objective function in (17), if there exist a scalar $\gamma(k)>0$, symmetric positive-definite matrices Q and P, and a matrix Y of appropriate dimension, satisfying the following convex optimization problem

$$\min_{\gamma \in Y} \gamma \tag{21}$$

subject to

$$\begin{bmatrix} 1 & e(k|k)^T \\ e(k|k) & Q \end{bmatrix} \succeq 0 \tag{22}$$

$$\begin{bmatrix} Q & \star & \star & \star & \star \\ C_e \mathcal{A}(\mathbf{p}(k)) C_e^{\dagger} Q + C_e \mathcal{B}(\mathbf{p}(k)) Y & Q & \star & \star \\ Q_1^{1/2} Q & 0 & \gamma I & \star \\ R^{1/2} Y & 0 & 0 & \gamma I \end{bmatrix} \succeq 0$$

where (\star) represents the symmetric expressions in the matrix.

Proof. The problem of minimizing the upper bound of the robust objective function can be expressed as $\min_{\{\gamma,P\}} \gamma$ subject to $e^T(k|k)Pe(k|k) < \gamma$. By defining $Q = \gamma P^{-1}$, and applying the Schur complement, this inequality can be transformed into the LMI in (22). To ensure the robust performance, the feedback control law $\Delta u(k+i|k) = Ke(k|k)$ must satisfy (18). Subsequently, plugging this control input, along with Lyapunov function (17) and error dynamics (14), into the stability constraint (18) yields

$$\mathcal{X}(k+i|k)^T \{ [C_e \mathcal{A}(\mathbf{p}(k)) + C_e \mathcal{B}(\mathbf{p}(k)) K C_e]^T$$

$$P[C_e \mathcal{A}(\mathbf{p}(k)) + C_e \mathcal{B}(\mathbf{p}(k)) K C_e] - C_e^T P C_e$$

$$+ C_e^T Q_1 C_e + C_e^T K^T R K C_e \} \mathcal{X}(k+i|k) \leq 0$$
 (24)

This inequality holds for every $i \ge 0$, if

$$[C_e \mathcal{A}(\mathbf{p}(k)) + C_e \mathcal{B}(\mathbf{p}(k)) K C_e]^T$$

$$P[C_e \mathcal{A}(\mathbf{p}(k)) + C_e \mathcal{B}(\mathbf{p}(k)) K C_e]$$

$$- C_e^T P C_e + C_e^T Q_1 C_e + C_e^T K^T R K C_e \leq 0 \quad (25)$$

Pre- and post-multiplying the above inequality by the Moore-Penrose pseudoinverse of matrix C_e , denoted by C_e^{\dagger} , gives

$$[C_e \mathcal{A}(\mathbf{p}(k)) C_e^{\dagger} + C_e \mathcal{B}(\mathbf{p}(k)) K]^T$$

$$P[C_e \mathcal{A}(\mathbf{p}(k)) C_e^{\dagger} + C_e \mathcal{B}(\mathbf{p}(k)) K]$$

$$- P + Q_1 + K^T RK \leq 0. \quad (26)$$

Next, substituting $P = \gamma Q^{-1}$ and Y = KQ, and pre- and post-multiplying by Q results in the LMI (23), which is affine in $[\mathcal{A}(\mathbf{p}(k)) \ \mathcal{B}(\mathbf{p}(k))]$. Therefore, it is satisfied for all $[\mathcal{A}(\mathbf{p}(k)) \ \mathcal{B}(\mathbf{p}(k))] \in \mathbf{\Omega}$ if and only if there exist $Q \succ 0$, Y = KQ and γ such that

$$\begin{bmatrix} Q & \star & \star & \star & \star \\ C_e \mathcal{A}_j(\mathbf{p}(k)) C_e^{\dagger} Q + C_e \mathcal{B}_j(\mathbf{p}(k)) Y & Q & \star & \star \\ Q_1^{1/2} Q & 0 & \gamma I & \star \\ R^{1/2} Y & 0 & 0 & \gamma I \end{bmatrix} \succeq 0.$$
(27)

VI. SIMULATION RESULTS

This section focuses on closed-loop simulation results of using the proposed robust MPC on an RF-excited APPJ in Argon using a validated physics-based model [7]. The states and inputs of the system are as follows

$$x = \begin{bmatrix} T_s & T_g \end{bmatrix}^T, \quad u = \begin{bmatrix} p & q \end{bmatrix}^T,$$
 (28)

where T_s and T_g denote the surface and gas temperature, while p and q represent the applied electric power and gas flow rate, respectively. In this study, the primary control objective is to ensure that the surface temperature closely follows a desired trajectory. Consequently, the control output is selected as $y = T_s$. Moreover, it is desirable for the states and the inputs to lie in the regions defined by [19]

$$\begin{bmatrix} 25 \text{ °C} \\ 20 \text{ °C} \end{bmatrix} \le \begin{bmatrix} T_s \\ T_q \end{bmatrix} \le \begin{bmatrix} 42.5 \text{ °C} \\ 80 \text{ °C} \end{bmatrix}, \tag{29a}$$

$$\begin{bmatrix} 1.5 \text{ W} \\ 1.0 \text{ slm} \end{bmatrix} \le \begin{bmatrix} p \\ q \end{bmatrix} \le \begin{bmatrix} 8.0 \text{ W} \\ 6.0 \text{ slm} \end{bmatrix}. \tag{29b}$$

Our simulation results clearly demonstrated that selecting the system states as scheduling variables effectively captures the system's nonlinear behavior. This choice empowers the control algorithm to dynamically adjust to the system dynamics and complex nature, thereby enhancing its accuracy and responsiveness to changes in operating conditions.

The LPV-SS model was trained using BNNs. To generate the dataset $\mathcal{D}=\{(\mathrm{p}(i),x(i),u(i)),(x(i+1))\}_{i=0}^{N-1}$ for system identification, open-loop simulations were conducted on a dynamic model consisting of a differential-algebraic system of equations [7]. In these simulations, the variables of interest, namely p and q, were manipulated as depicted in Fig. 1a, and the resulting states were recorded as illustrated in Fig. 1b. A partition of 65% of the dataset was designated as the training set, while the remaining portion was allocated to the testing set.

The matrices A and B were modeled using three fully-connected DenseVariational layers, each comprising 4 hidden units. The hidden layers utilized the linear activation function, while no activation function was applied to the output layers. The tuning parameters were set as $\rho_m=0.5$, $\sigma_1=1.5$, and $\sigma_2=1$. Additionally, the ADAM optimizer with exponential decay, featuring a decay rate of 0.9, was utilized. In assessing the accuracy of the LPV-SS model, the Best Fit Rate (BFR) was computed as $BFR(\theta)=$

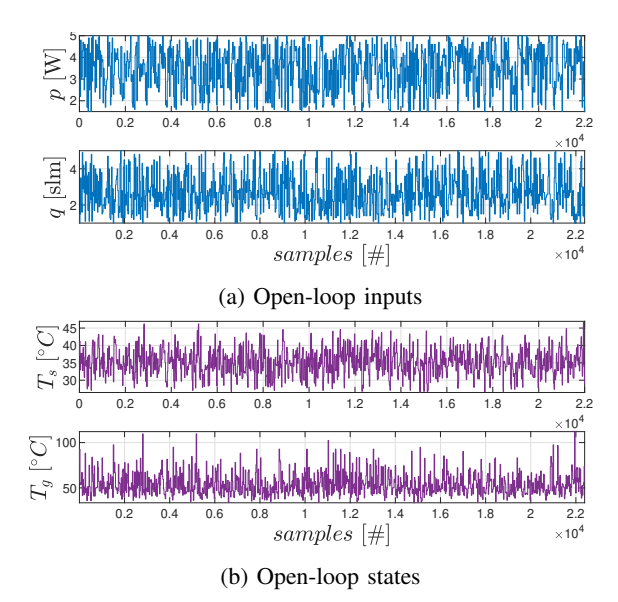


Fig. 1: Dataset used for LPV-SS model learning.

TABLE I: BFR accuracy criterion for the trained LPV-SS model.

Dataset	T_s	T_g
Training set	95.49%	87.61%
Testing set	94.75%	86.31%

 $100\%.\max_k\left(1-\frac{\|x_{k+1}-\hat{x}_{k+1}(\theta)\|_2}{\|x_{k+1}-\bar{x}_{k+1}\|_2},0\right)$ with the corresponding results presented in Table I.

A comparison between the actual training and testing states and their predicted mean values, along with their confidence intervals spanning $[\mu_{\hat{x}}-5\sigma_{\hat{x}},\mu_{\hat{x}}+5\sigma_{\hat{x}}]$ across 500 samples are illustrated in Fig. 2. Additionally, the percentage of datasets falling within the confidence interval is given in Table II.

Furthermore, at each time step, we randomly sample $N_{MC}=50$ models to evaluate the mean and standard deviation of $A(\cdot)$ and $B(\cdot)$. Fig. 3 demonstrates the evolution of the entries of these LPV-SS matrices across 500 sampling instants, along with their corresponding uncertainty range.

The primary control objective is to ensure precise tracking of the surface temperature along a desired trajectory. To evaluate the performance of the LPV-based robust controller, we conducted an additional simulation, comparing it with an alternative control scheme. The alternative was a baseline MPC controller that used an LTI model of the APPJ system obtained with subspace identification in [20].

For the MPC controller, both the prediction horizon and control horizon were set to $n_p = n_c = 5$, utilizing a quadratic

TABLE II: Percentage of data within the confidence interval.

Dataset	T_s	T_g
Training set	98.72%	93.08%
Testing set	97.19%	92.55 %

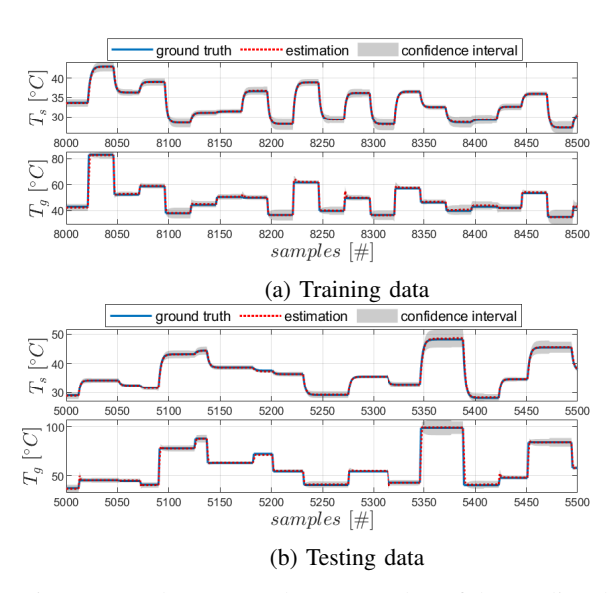


Fig. 2: Actual states vs. the mean value of the predicted states within the confidence interval.

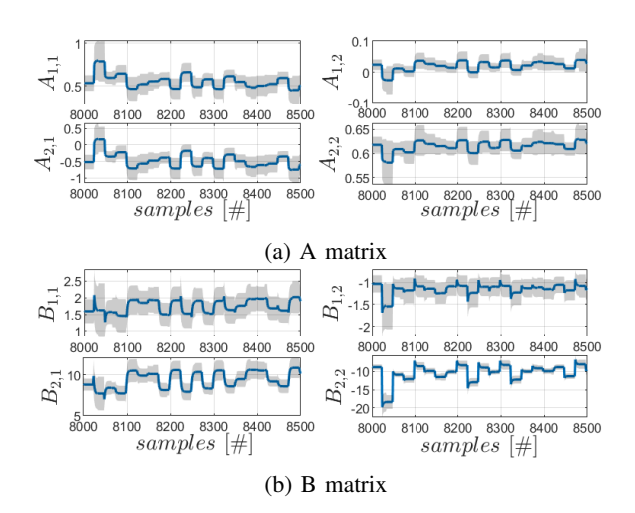


Fig. 3: Some entries of A and B matrices and their corresponding confidence intervals.

cost function as $J(k) = \sum_{i=0}^{n_p} \left(\|e(k+i|k)\|_{Q_1}^2 + \|\Delta u(k+i|k)\|_R^2 \right)$. To illustrate the robustness of the control strategies against disturbances, the tip-to-surface distance of the APPJ was intentionally increased to 6 [mm] at t=25 [sec], before reverting to its initial value of 4 [mm] at t=35 [sec]. Closed-loop simulation results depicted in Fig. 4 indicate that the robust MPC controller in the LPV framework effectively tracks the desired trajectory with high precision. Conversely, the MPC controller utilizing the LTI model exhibits a faster transient response; however, it suffers from persistent offset errors attributed to modeling discrepancies. Furthermore, during disturbance occurrences, the robust controller adeptly mitigates the effects, whereas the performance of the MPC controller significantly deteriorates.

The comparison of control inputs between the two controllers is illustrated in Fig. 5. Evidently, both controllers maintain control inputs within the admissible

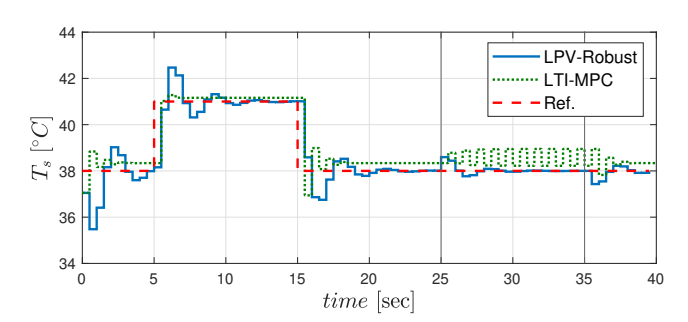


Fig. 4: Tracking performance of the proposed robust LPV controller compared to the baseline MPC.

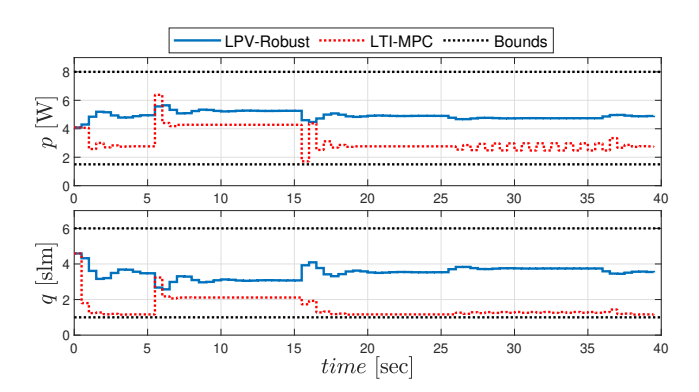


Fig. 5: Control efforts of the proposed robust LPV controller compared to the baseline MPC.

range. Nonetheless, the robust-LPV control scheme demands greater electric power and gas flow rate resulting in a superior tracking performance albeit at the expense of heightened control efforts.

VII. CONCLUSIONS

This work proposed a robust control design approach in the LPV framework for atmospheric pressure plasma jets (APPJs). A state-space LPV model of the system was learned using Bayesian neural networks, which allowed capturing the complex and nonlinear dynamics of the APPJs while also providing statistical information about the uncertainty in the learned LPV model. The LPV-SS model and the associated uncertainty set were then utilized for the robust control design, which involved solving an optimization problem with LMI constraints that aimed at minimizing the upper limit on the robust performance objective. Simulation results illustrated that the developed data-driven LPV model accurately described the APPJs dynamics. Additionally, the robust predictive controller effectively addressed the effects of modeling mismatch arising from the learned LPV-SS model, as well as external disturbances. Comparative assessments with an alternative control scheme, which also was a model predictive controller, highlighted the superior robustness and tracking performance achieved by the LPVbased design approach.

REFERENCES

[1] D. Gidon, H. S. Abbas, A. D. Bonzanini, D. B. Graves, J. M. Velni, and A. Mesbah, "Data-driven lpv model predictive control of

- a cold atmospheric plasma jet for biomaterials processing," *Control Engineering Practice*, vol. 109, p. 104725, 2021.
- [2] D. Rodrigues, K. J. Chan, and A. Mesbah, "Data-driven adaptive optimal control under model uncertainty: an application to cold atmospheric plasmas," *IEEE Transactions on Control Systems Technology*, vol. 31, no. 1, pp. 55–69, 2022.
- [3] H. B. Baniya, R. P. Guragain, B. Baniya, and D. P. Subedi, "Experimental study of cold atmospheric pressure plasma jet and its application in the surface modification of polypropylene," *Reviews of Adhesion and Adhesives*, vol. 8, no. 2, pp. S1–S14, 2020.
- [4] L. Minati, C. Migliaresi, L. Lunelli, G. Viero, M. Dalla Serra, and G. Speranza, "Plasma assisted surface treatments of biomaterials," *Biophysical Chemistry*, vol. 229, pp. 151–164, 2017.
- [5] M. J. Nicol, T. R. Brubaker, B. J. Honish, A. N. Simmons, A. Kazemi, M. A. Geissel, C. T. Whalen, C. A. Siedlecki, S. G. Bilén, S. D. Knecht, et al., "Antibacterial effects of low-temperature plasma generated by atmospheric-pressure plasma jet are mediated by reactive oxygen species," *Scientific reports*, vol. 10, no. 1, p. 3066, 2020.
- [6] P. Lin, J. Zhang, T. Nguyen, V. M. Donnelly, and D. J. Economou, "Numerical simulation of an atmospheric pressure plasma jet with coaxial shielding gas," *Journal of Physics D: Applied Physics*, vol. 54, no. 7, p. 075205, 2020.
- [7] D. Gidon, D. B. Graves, and A. Mesbah, "Effective dose delivery in atmospheric pressure plasma jets for plasma medicine: A model predictive control approach," *Plasma Sources Science and Technology*, vol. 26, no. 8, p. 085005, 2017.
- [8] Y. Bao, K. J. Chan, A. Mesbah, and J. M. Velni, "Learning-based adaptive-scenario-tree model predictive control with probabilistic safety guarantees using bayesian neural networks," in 2022 American Control Conference (ACC), pp. 3260–3265, IEEE, 2022.
- [9] J. Mohammadpour and C. W. Scherer, Control of linear parameter varying systems with applications. Springer Science & Business Media, 2012.
- [10] Y. Bao and J. M. Velni, "An overview of data-driven modeling and learning-based control design methods for nonlinear systems in lpv framework," in *Proc. of the 5th IFAC Workshop on Linear Parameter* Varying Systems, 2022.
- [11] F. Berkenkamp and A. P. Schoellig, "Safe and robust learning control with gaussian processes," in 2015 European Control Conference (ECC), pp. 2496–2501, IEEE, 2015.
- [12] F. Liang, "Bayesian neural networks for nonlinear time series forecasting," Statistics and computing, vol. 15, pp. 13–29, 2005.
- [13] C. Blundell, J. Cornebise, K. Kavukcuoglu, and D. Wierstra, "Weight uncertainty in neural network," in *International conference on machine learning*, pp. 1613–1622, PMLR, 2015.
- [14] T. Hastie, R. Tibshirani, J. Friedman, T. Hastie, R. Tibshirani, and J. Friedman, "Model assessment and selection," *The elements of statistical learning: data mining, inference, and prediction*, pp. 219–259, 2009.
- [15] D. M. Blei, A. Kucukelbir, and J. D. McAuliffe, "Variational inference: A review for statisticians," *Journal of the American statistical Association*, vol. 112, no. 518, pp. 859–877, 2017.
- [16] T. Kato and H.-H. Lee, "Tracking and constant disturbance rejection of robust constrained LMI-based MPC," *IEEJ Transactions on Elec*tronics, Information and Systems, vol. 130, no. 12, pp. 2219–2226, 2010.
- [17] B. Kiumarsi, F. L. Lewis, M.-B. Naghibi-Sistani, and A. Karimpour, "Optimal tracking control of unknown discrete-time linear systems using input-output measured data," *IEEE transactions on cybernetics*, vol. 45, no. 12, pp. 2770–2779, 2015.
- [18] M. V. Kothare, V. Balakrishnan, and M. Morari, "Robust constrained model predictive control using linear matrix inequalities," *Automatica*, vol. 32, no. 10, pp. 1361–1379, 1996.
- [19] A. D. Bonzanini, J. A. Paulson, G. Makrygiorgos, and A. Mesbah, "Fast approximate learning-based multistage nonlinear model predictive control using gaussian processes and deep neural networks," *Computers & Chemical Engineering*, vol. 145, p. 107174, 2021.
- [20] D. Gidon, B. Curtis, J. A. Paulson, D. B. Graves, and A. Mesbah, "Model-based feedback control of a khz-excited atmospheric pressure plasma jet," *IEEE Transactions on Radiation and Plasma Medical Sciences*, vol. 2, no. 2, pp. 129–137, 2017.